Journal of Alloys and Compounds 504 (2010) 468–474

Contents lists available at ScienceDirect

Journal of Alloys and Compounds

journal homepage: www.elsevier.com/locate/jallcom

Optical band gap, glass transition temperature and structural studies of $(100-2x)TeO_2$–xAg_2O–xWO_3 glass system

G. Upender[a,*], S. Ramesh[a], M. Prasad[a], V.G. Sathe[b], V.C. Mouli[a]

[a] Department of Physics, Osmania University, Hyderabad 500 007, India
[b] UGC-DAE CSR, Khandwa Road, Indore 452 017, India

ARTICLE INFO

Article history:
Received 4 December 2009
Received in revised form 31 May 2010
Accepted 1 June 2010
Available online 11 June 2010

Keywords:
Amorphous materials
Optical absorption
DSC
Raman spectroscopy

ABSTRACT

Optical absorption, differential scanning calorimetry (DSC) and Raman studies have been carried out on $(100-2x)TeO_2$–xAg_2O–xWO_3 ($7.5 \le x \le 30$) glass system. The Raman spectra showed that the structure of glass network consists of $[TeO_4]$, $[TeO_3]/[TeO_{3+1}]$, $[WO_4]$ units. The glass transition temperature (T_g) values were measured from DSC thermogram and the variation in T_g has been discussed in terms of physical parameters like number of bonds per unit volume (n_b), average cross-link density ($\overline{n_c}$), average stretching force constant ($\overline{F}$), oxygen molar volume (V_o) and oxygen packing density (OPD) values. The cut-off wavelength (λ_c), optical band gap (E_{opt}), Urbach energy (ΔE) and refractive index (n) values were calculated from optical absorption data. The observed decrease in optical band gap (E_{opt}), Urbach energy (ΔE) and increase in refractive index (n) values have been discussed in terms of structural changes brought about by WO_3 and Ag_2O incorporation in to TeO_2 network.

1. Introduction

Currently heavy metal oxide, fluoride, and oxyfluoride glasses receive considerable attention in view of their potential for use as laser hosts, in fiber optics and as non-linear optical materials [1–3]. Tellurium oxide based glasses attracted the scientific community due to their application in the field of glass ceramics, solid state batteries and fuel cells, optical amplifiers and non-linear optical devices [4,5]. These glasses have low phonon energy [6], large third-order non-linear susceptibility [7], low melting temperature [8], low glass transition temperature, low crystallization ability [9], good chemical resistance [10], good transmission for infrared rays with a wide range of wavelength [11], high dielectric constants [12] and large refractive indices [13]. For these reasons, tellurite glasses have become the subject of thorough investigations. Raman, IR spectra, some optical properties and MDSC study of TeO_2–WO_3 and TeO_2–WO_3–PbO glasses have been published by Upender et al. [14,15]. A survey of the literature indicates that reports on the physical and optical properties of TeO_2 glasses containing WO_3 and Ag_2O are limited. In view of these, we have carried out Optical absorption, Raman and DSC studies on TeO_2–Ag_2O–WO_3 glass system.

The present paper reports the short-range structure, DSC and optical properties of TeO_2–Ag_2O–WO_3 glass system. The variation in T_g has been compared with physical and structural properties such as OPD, oxygen molar volume (V_o), number of bonds per unit volume (n_b), average cross-link density ($\overline{n_c}$) and average stretching force constant ($\overline{F}$). The optical properties such as the optical band gap (E_{opt}), Urbach energy (ΔE), refractive index (n) have been correlated with the Raman spectral studies of these glasses.

2. Experimental

The glasses used for the present study were prepared by the melt quenching technique. The starting materials used in the present study were analar grade TeO_2 (99.9% purity), Ag_2O (99.9% purity), WO_3 (99.9% purity). The chemicals were weighed to get the required composition and ground in a mortar with a pestle for 1 h to obtain homogeneous mixtures. The compositions of glasses used in the present study were $(100-2x)TeO_2$–xAg_2O–xWO_3 (where $x = 7.5$, 15, 22.5, 30). Each batch was then transferred to a platinum crucible and melted at about 750–850 °C in an electric furnace. This melt was held at this temperature for 30 min until a bubble free liquid was formed. The melts were stirred from time to time to ensure complete homogeneity and were then poured on a pre-heated stainless steel mould containing circular holes and pressed with another steel disc. The prepared samples were subsequently annealed for 12 h at 150 °C in another furnace to relieve the mechanical strains. The compositions of the glass samples employed in these studies are given in Table 1.

X-ray diffractograms of powdered glass samples were recorded using a copper target ($k_\alpha = 1.54$ Å) on a Philips PW (1140) diffractometer at room temperature.

The densities of glasses were determined at room temperature by the Archimedes method using xylene ($\rho = 0.86$ g/cc) as the immersion liquid. Repeated densities measurements were agreed within ±0.01%. From these density values, the molar volume of glasses ($V_m = \Sigma x_i M_i/\rho$) and the molar volume of oxygen (volume of glass in which 1 mole of oxygen is contained, $V_o = (\Sigma x_i M_i/\rho)(1/\Sigma x_i n_i)$ were calculated. x_i is the molar fraction of each component i, M_i is the molecular weight, ρ is the glass density and n_i is the number of oxygen atoms in each oxide. Oxygen packing density (OPD) of each glass was calculated from the density and composition using the formula OPD = 1000C (ρ/M), C is the number of oxygens per formula unit.

* Corresponding author. Tel.: +91 40 27682242; fax: +91 40 27099020.
E-mail address: upender_b4u@yahoo.co.in (G. Upender).

0925-8388/$ – see front matter © 2010 Elsevier B.V. All rights reserved.
doi:10.1016/j.jallcom.2010.06.006

Table 1
Glass compositions and the Raman band positions of the glass system $(100-2x)TeO_2$–xAg_2O–xWO_3, with errors ± 1 cm^{-1}.

Sample ID	Composition (mol%)	Raman shift δ ± 1 (cm^{-1})					
TAW1	$85TeO_2$–$7.5Ag_2O$–$7.5WO_3$	342	459	666	764	823	916
TAW2	$70TeO_2$–$15Ag_2O$–$15WO_3$	344	475	702	775	835	908
TAW3	$55TeO_2$–$22.5Ag_2O$–$22.5WO_3$	355	485	730	–	839	905
TAW4	$40TeO_2$–$30Ag_2O$–$30WO_3$	360	496	735	–	843	898

Raman spectra of the present glass samples were recorded at room temperature using JOBIN–YVON HORIBA (LABRAM HR-800), spectrometer in the wavenumber range 200–1050 cm^{-1}. The excitation wavelength used was 632.81 nm (He–Ne laser), with a power of 9 mW. The incident laser power is focused in a diameter of ~1–2 μm and a notch filter is used to suppress Rayleigh light. Samples used for the measurement were of 1 mm thickness and 1 cm in diameter. Raman shifts are measured with a precision of ~0.3 cm^{-1} and the spectra resolution is of the order 1 cm^{-1}.

The glass transition temperature (T_g) was measured using a temperature modulated differential scanning calorimeter (TA Instruments, DSC 2910). All samples were heated at the standard rate of 10 °C min^{-1} in aluminum pans.

Optical absorption spectra of all the glass samples (≈1 mm thick) were recorded on a double beam Shimadzu UV-3100 spectrometer in the wavelength range 350–800 nm at room temperature using air as the reference medium. The uncertainty in the observed wavelength is about ±1 nm.

3. Results and discussion

3.1. XRD, density, molar volume, OPD and oxygen molar volume

The short and medium range orders in the $(100-2x)TeO_2$–xAg_2O–xWO_3 glass system structure were tested by means of X-ray diffraction. The obtained diffraction pattern (Fig. 1) of all the samples showed a broad hump over the region 20–35° for 2θ values, which is characteristic of the glass structure for these samples. The measured density (ρ), molar volume (V_m), oxygen packing density (OPD) and oxygen molar volume (V_o) of the glass samples are given in Table 2. The densities of glasses in the $(100-2x)TeO_2$–xAg_2O–xWO_3 system vary between 5.903 and 6.593 g/cc for the glasses $85TeO_2$–$7.5Ag_2O$–$7.5WO_3$ (TAW1) and $40TeO_2$–$30Ag_2O$–$30WO_3$ (TAW4), respectively. The density values of the present glasses are greater than the density for pure TeO_2 glass (5.67 g/cc) [16], and agree with the data reported elsewhere [17]. From Fig. 2 it is found that the density (ρ) increases and molar volume (V_m) also increases as the WO_3–Ag_2O proportion increases, at the expense of the TeO_2 content. The increase in the values of density is attributed to the higher molecular weight of WO_3 (231.84 g/mol) and Ag_2O (231.74 g/mol) in comparison with that of the TeO_2 (159.6 g/mol) and it also related to change in their atomic radii (Te = 0.70 Å, W = 0.62 Å and Ag = 1.26 Å) [17]. In general, it is expected that the density and the molar volume should show opposite behaviour to each other, but in

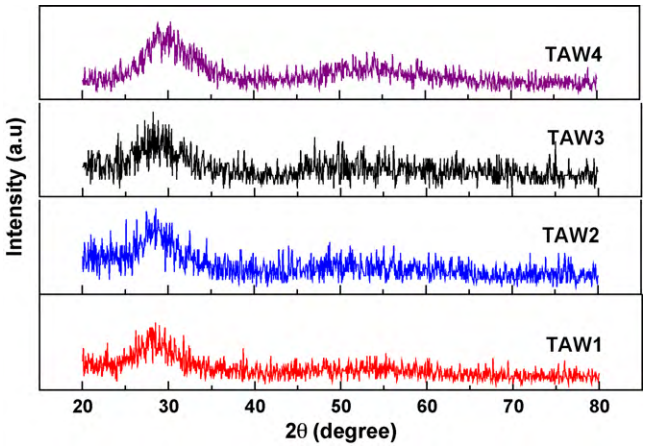

Fig. 1. XRD patterns of TeO_2–Ag_2O–WO_3 glasses.

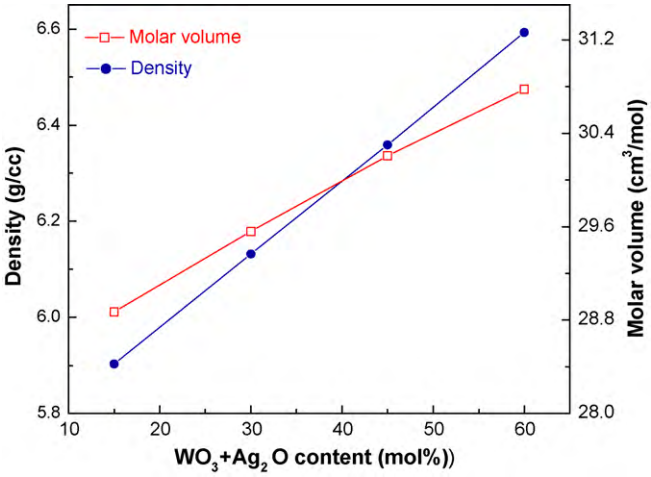

Fig. 2. Variation of the density and the molar volume of glasses as a function of the WO_3–Ag_2O content.

Table 2
Physical and optical parameters of the glass system $(100-2x)TeO_2$–xAg_2O–xWO_3.

Parameter	x = 7.5	x = 15	x = 22.5	x = 30
Average molecular weight (g/mol)	170.429	181.257	192.086	202.914
Density, ρ (g/cc)	5.903	6.132	6.359	6.593
Molar volume, V_m (cm^3/mol)	28.872	29.559	30.207	30.777
Oxygen packing density (mol/l)	69.271	67.661	66.209	64.994
Oxygen molar volume, V_o (cm^3/mol)	14.436	14.779	15.104	15.386
Glass transition temperature, T_g (°C)	287	276	273	271
Onset crystallization, T_o (°C)	375	346	365	352
Thermal stability, ΔT (°C)	88	70	92	81
Average cross-linking density ($\overline{n_c}$)	1.72	1.48	1.27	1.08
Number of bonds per unit volume (10^{28} m^{-3})	8.34	8.15	7.98	7.83
Average stretching force constant, $\overline{F}$(N/m)	215.10	214.47	213.91	213.21
Cut-off wavelength, λ (nm)	404	436	449	580
Optical band gap, E_{opt} (eV)	2.47	2.45	2.36	2.01
Urbach energy, ΔE (eV)	0.37	0.29	0.26	0.15
Optical basicity (Λ_{th})	0.927	0.894	0.861	0.828
Refractive index (n)	2.55	2.56	2.59	2.73

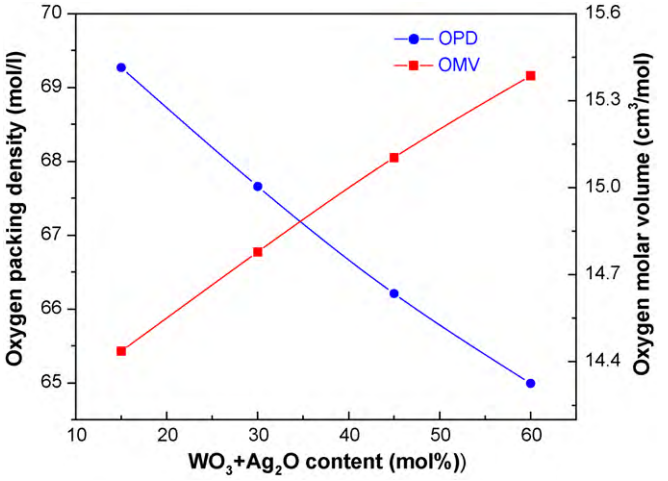

Fig. 3. Variation of the oxygen packing density (OPD) and the oxygen molar volume (V_o) of glasses as a function of the WO_3–Ag_2O content.

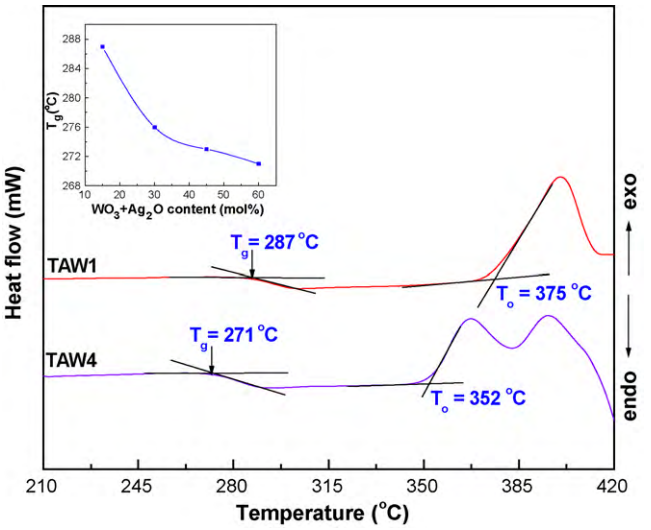

Fig. 4. DSC curves of $85TeO_2$–$7.5Ag_2O$–$7.5WO_3$ and $40TeO_2$–$30Ag_2O$–$30WO_3$ glasses. Heating rate was 10 °C/min.

the present glass system the behaviour is different. However, this anomalous behaviour was reported earlier for many glass systems, for example, TeO_2–Nb_2O_5–Bi_2O_3 [18], TeO_2–Na_2O–B_2O_3 [19] and Bi_2O_3–Li_2O–ZnO–B_2O_3 [20]. The molar volume behaviour reveals that an increase in the WO_3–Ag_2O content leads to the formation of non-bridging oxygens (NBOs) and opens up the structure of the glasses. From Fig. 3 and Table 2, it is found that oxygen packing density (OPD) values decrease from 69.271 to 64.994 mol/l, the oxygen molar volume (V_o) increases from 14.436 to 15.386 cm^3/mol. Hence the network is more open and the network becomes less tightly packed. This behaviour could be explained taking into account that the substitution of TeO_2 mol by mol by WO_3–Ag_2O content, two silver atoms and one tungsten atom are introduced, while the number of oxygen atoms are same according to the ratio 4/4. The large value of the radii (1.26 Å) and bond length (2.549 Å) of Ag_2O [21] compared to those of WO_3 and TeO_2, resulted in a formation of excess free volume, which increases the overall molar volume of these glasses. This supports the variation in OPD and V_o values.

3.2. Glass transition temperature (T_g)

The DSC curves of TAW1 and TAW4 glasses scanned at a rate of 10 °C min^{-1} are shown in Fig. 4. Each DSC scan exhibits a small endothermic peak corresponding to the glass transition temperature, T_g, at 287 °C for the $85TeO_2$–$7.5Ag_2O$–$7.5WO_3$ (TAW1) and at 271 °C for the $40TeO_2$–$30Ag_2O$–$30WO_3$ (TAW4) glass. Thermal parameters such as the glass transition temperature (T_g), onset crystallization (T_o) and thermal stability ($\Delta T = T_o - T_g$) for different glass compositions prepared in TeO_2–Ag_2O–WO_3 system are given in Table 2. It is well known from the literature that when TeO_2 is substituted by WO_3 yields an increase in T_g this is due to stronger W–O bond than the Te–O bond (bond enthalpies are 672 and 376 kJ/mol, respectively) [22] and the cross-link density for TeO_2 is 2 whereas it is 3 for WO_3 [23]. Hence it is obvious that when a higher bond strength and a higher cross-link substance substitutes for a lower one, the mean bond strength and network connectivity increases resulting in the increase of T_g. But in the present glass system the substitution of TeO_2 by WO_3–Ag_2O content causes a slight decrease in T_g, this is contrary to above result. This can be understood as follows: when WO_3–Ag_2O content increases, due to Ag_2O content rather than WO_3, the glass network becomes more open and this suggests that the addition of Ag_2O creates more non-bridging oxygens, moreover the Ag^+ ions with larger ion size as compared to Te^{4+} and W^{6+} would eventually form loosened glassy network, and thus Ag_2O is the most contributing oxide to decrease the T_g. On the other hand, the decrease in T_g may be ascribed due to lower the bond enthalpy of Ag–O (155 kJ/mol) as compared to bond enthalpies of Te–O and W–O.

The glass transition temperature (T_g) depends on a number of parameters. It is more informative for analyzing the glass network to correlate data between thermal and structural properties, e.g., between (T_g) and average cross-link density ($\overline{n_c}$), number of bonds per unit volume (n_b) and the average stretching force constant ($\overline{F}$).

The average cross-link density ($\overline{n_c}$) of the glass is calculated using the relationship [24–26].

$$\overline{n_c} = \frac{\left[\sum_i x_i (n_c)_i (N_c)_i\right]}{\sum_i x_i (N_c)_i} \quad (1)$$

where x_i is mole fraction; n_c is number of cross-links per cations and is equal to the number of bonds minus two; N_c is number of cations per glass formula unit.

The increase of WO_3–Ag_2O content at the expense of TeO_2 from $2x$ = 15–60 mol% leads to decrease in the average cross-link density from 1.72 to 1.08 as shown in Table 2.

The number of bonds per unit volume (n_b) of the glass is calculated using the relationship [24–26].

$$n_b = \frac{N_A}{V_m} \sum_i \left(n_f x\right)_i \quad (2)$$

where N_A is Avogadro's number; V_m is molar volume; n_f is coordination number of the cation; x is mole fraction. The coordination numbers of W, Ag, and Te are 6, 2 and 4, respectively. The value of n_b for pure TeO_2 is 7.74×10^{28} m^{-3} [27]. The number of bonds per unit volume of the present glass system is found to decrease from 8.34×10^{28} to 7.83×10^{28} m^{-3} with increasing WO_3–Ag_2O content as shown in Table 2.

Average stretching force constant ($\overline{F}$) of the glass is calculated using the relationship [24–26].

$$\overline{F} = \frac{\sum_i x_i (n_f) F_i}{\sum_i x_i (n_f)_i} \quad (3)$$

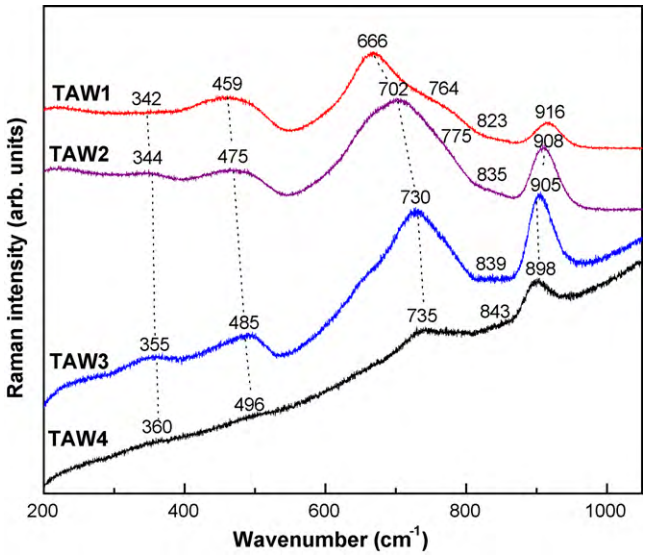

Fig. 5. Raman spectra at room temperature of TeO_2–Ag_2O–WO_3 glasses.

where n_f is coordination number of the cation; x_i is mole fraction and F_i is given by

$$F_i = \frac{17}{r^3} \quad (4)$$

where F_i is the stretching force constant of oxide and i denotes the component oxide, and r is the bond length between cation and anion. The average stretching force constant of the bond Te–O is 216 N/m [27]. The average stretching force constant ($\overline{F}$) of the present glass system is found to decrease from 215.10 to 213.21 N/m with increasing WO_3–Ag_2O content (Table 2). Therefore the decrease in T_g of the present glass system can be ascribed due to the decrease in average cross-link density ($\overline{n_c}$), number of bonds per unit volume (n_b) and average stretching force constant ($\overline{F}$). The observed decrease in T_g of the present glass system with increase of WO_3–Ag_2O content in the glass matrix, as shown in inset of Fig. 4 is also ascribed to some structural changes such as transformation of some TeO_4 tbp units with bridging oxygen (BO) into TeO_3 tp units with NBO via TeO_{3+1}. The observed variation in oxygen packing density (OPD) and oxygen molar volume (V_o) values can also be correlated to the decrease in T_g. The glass transition temperature (T_g) is a measure of the strength of a material [28]. Hence, from DSC results, it is concluded that the strength of the present glass system decreases with WO_3–Ag_2O content. The T_g of present glasses are lower than T_g of the glasses in TeO_2–WO_3 system [29] and higher than T_g of the glasses in TeO_2–Ag_2O system [30], TeO_2–Ag_2O–V_2O_5 system [31] and comparable to T_g of those found in [17].

3.3. Raman spectral studies

The Raman spectra of the glass samples $(100-2x)TeO_2$–xAg_2O–xWO_3 with $7.5 \le x \le 30$ mol% is shown in Fig. 5. The assignments of Raman bands are given in Table 3 and observed Raman band positions for all the compositions are summarized in Table 1. The deconvoluted Raman spectrum for the TAW1 is shown in Fig. 6. The Raman spectrum of TAW1 glass consists of six Raman bands (RB) at around 342 cm^{-1} (RB_{342}), 459 cm^{-1} (RB_{459}), 666 cm^{-1} (RB_{666}), 764 cm^{-1} (RB_{764}), 823 cm^{-1} (RB_{823}) and 916 cm^{-1} (RB_{916}). The RB_{459}–RB_{764} seems to be typical for tellurite matrix in various tellurite glasses: WO_3–TeO_2 [32], ZnO–Bi_2O_3–TeO_2 [33], PbO–WO_3–TeO_2 [34]. Hence, in accordance with [32–34] we assign observed RB as follows: (i) RB_{666} to symmetric stretch of Te–O bonds in TeO_4 trigonal bipyramidal units or to Te–O–Te linkage between two fourfold coordinated Te atoms. (ii) RB_{764} to stretching vibrations of Te–O bonds of TeO_3/TeO_{3+1} units. (iii) RB_{479} to the stretching vibrations of Te–O–W linkages. However, the RB_{459} was observed in many tellurite glasses and it is a signature of bending modes of Te–O–Te linkages. The Raman studies on tungsten tellurite glasses have shown that observed RB_{916} is assigned to symmetric stretching vibrations of W–O^- and W=O bonds associated with WO_4 or WO_6 units [17,35]. The RB_{823} is assigned to stretching vibrations of W–O–W in WO_4 or WO_6 units [17,35]. The RB_{342} is the characteristic bands of tungsten glasses which may be attributed to bending vibrations of W–O–W in the WO_6 units [17,35]. Equimolar substitution of TeO_2 by WO_3–Ag_2O causes significant changes in the Raman spectra arising from tungsten network and tellurite network (see Fig. 5). As WO_3–Ag_2O proportion increases up to $2x = 45$ mol%, the RB_{666} and RB_{764} gradually overlap and form a new RB_{730} and this RB_{730} is shifted to RB_{735} as WO_3–Ag_2O proportion increases up to $2x = 60$ mol%. The $RB_{730–735}$ is typical for tellurite glasses prepared from TeO_2 and heavy metal oxides and the $RB_{730–735}$ is assigned to symmetric stretching vibrations between Te and non-bridging oxygen (NBO) in TeO_{3+1} units (The TeO_{3+1} unit can be thought of a distorted trigonal bipyramidal (TeO_4) unit with one oxygen further away from the central tellurium than the remaining three oxygens) or possibly to stretching mode of TeO_3 unit [36] most likely to Te=O bond stretching in O=TeO_2 units [32]. As the WO_3–Ag_2O content increases from 15 to 60 mol%, the intensity of the RB_{459} decreases while this RB_{459} is shifted to higher frequencies (RB_{496}). This is expected result since there are fewer Te–O–Te linkages and more Te–O–W linkages [37]. This observation can also be

Table 3
Assignments of Raman bands of glass system $(100-2x)TeO_2$–xAg_2O–xWO_3.

Raman band (cm^{-1}) observed in the glass	Assignment
890–920	Stretching vibrations of W–O^- and W=O bonds in WO_4 or WO_6 units
820–850	Stretching vibrations of W–O–W in WO_4 or WO_6 units
340–360	Bending vibrations of W–O–W in WO_6 units
720–735	Stretching vibrations of TeO_3/TeO_{3+1} units
760–775	Stretching vibrations of TeO_3/TeO_{3+1} units
650–670	Stretching vibrations of TeO_4 units
440–496	Stretching vibrations of Te–O–W linkages

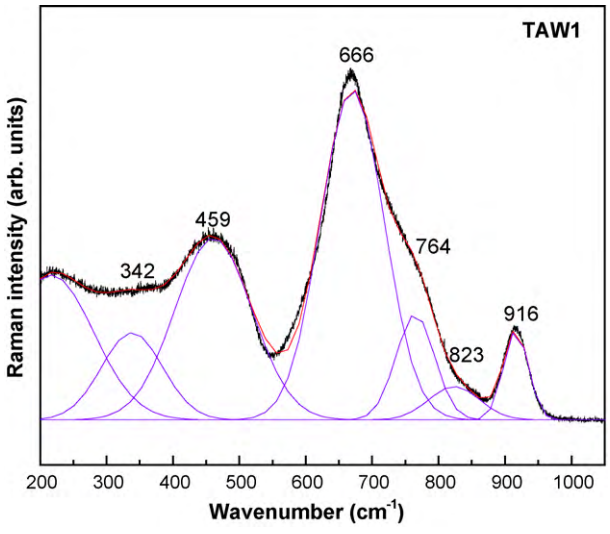

Fig. 6. The deconvolution of the Raman spectrum of $85TeO_2$–$7.5Ag_2O$–$7.5WO_3$ glass.

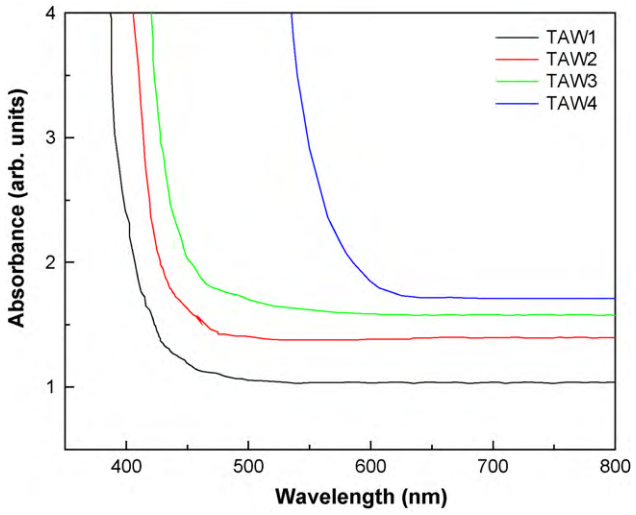

Fig. 7. Optical absorption spectra of TeO_2–Ag_2O–WO_3 glasses.

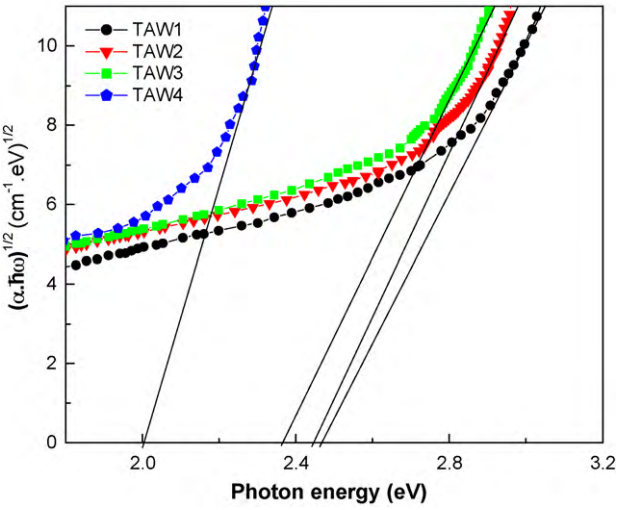

Fig. 8. $(\alpha\hbar\omega)^{1/2}$ as a function of $\hbar\omega$ for TeO_2–Ag_2O–WO_3 glasses.

explained as follows: as $WO_3 + Ag_2O/TeO_2$ mole fraction increases, NBOs are created both at equatorial and axial positions, leading to the formation of $Te{-}_{eq}O^-Ag^+$, $Te{-}_{ax}O^-Ag^+$ and also Te=O which in turn shifts the RB_{459} to higher frequencies. On the other hand, WO_3–Ag_2O content also creates a part of the NBO by modifying the W–O–W linkages with the structural units of the form, $W{-}O^-Ag^+$ and W=O. All these species prevents the formation of TeO_4 tbp units in all samples (TAW2–TAW4). These results are in agreement with the reported results [17].

As the WO_3–Ag_2O content increases from 15 to 60 mol%, the intensity of RB_{916} increases while this band is shifted to lower frequencies (RB_{898}). The observed shift in the RB_{916} band toward lower wave numbers and variation in the intensity of the bands is may be an indication of the decrease in bridging oxygens of WO_4 units and simultaneous increase in non-bridging oxygens of WO_4 units and also due to the bond between NBO and tungsten atoms is weakened and therefore, the vibration appears in the lower wave number region.

The intensity of the RB_{823} changes and it shifts to RB_{843} with the content of WO_3–Ag_2O up to 60 mol%. The intensity of the RB_{342} increases and it shifts to RB_{355} as the WO_3–Ag_2O content increases from 15 to 45 mol% and after its intensity decreases and shifts to RB_{360} as WO_3–Ag_2O content increases up to 60 mol%. All these observations suggest that the addition of WO_3–Ag_2O content causes continuous structural transition in TeO_2 through the continuation creation of non-bridging oxygens in the form of $Te{-}_{eq}O^-Ag^+$, $Te{-}_{ax}O^-Ag^+$, Te=O, $W{-}O^-Ag^+$ and W=O. On the other hand, both W^{6+} and Ag^+ are heavy metal ions; therefore WO_3–Ag_2O addition to the glass may distort and strain the TeO_2 network.

3.4. Optical properties

3.4.1. Optical band gap (E_{opt}) and Urbach energy (ΔE)

The study of optical absorption edge is a useful information for understanding the optically induced transitions and optical band gaps of materials. The principle of the technique is that a photon with energy greater than the band gap energy will be absorbed. There are two kinds of optical transitions at the fundamental absorption edge: direct and indirect transitions, both of which involve the interaction of an electromagnetic wave with an electron in the valence band. Fig. 7 shows the optical absorption spectra of TeO_2–Ag_2O–WO_3 glasses recorded at room temperature in the wavelength region 350–800 nm. A distinct cut-off wavelength (λ_c) was observed for each glass sample and the λ_c values are presented in Table 2. From Table 2, it is clear that λ_c observed at 404 nm for TAW1 glass is found to be shifted gradually towards higher wavelength side (red shifted) with increase in the WO_3–Ag_2O content (580 nm for TAW4).

The absorption coefficient α (ω) near the fundamental absorption edge of each spectrum shown in Fig. 7 was determined at wavelength intervals of 2.5 nm in the non-linear region and 5 nm for the linear region, from the following relation [38].

$$\alpha(\omega) = \left(\frac{1}{t}\right) \ln\left(\frac{I}{I_o}\right) \tag{5}$$

where t is the thickness of each sample and $\ln(I/I_o)$ corresponds to absorbance.

The relation between $\alpha(\omega)$ and photon energy of the incident radiation, $\hbar\omega$ is given by the following relation [39].

$$\alpha(\omega) = \frac{A(\hbar\omega - E_{opt})^p}{\hbar\omega} \tag{6}$$

where E_{opt} is the optical band gap energy in eV (the optical band gap in amorphous system is closely related to the energy gap between the valence band and conduction band), A is a constant and p is an index which can be assumed to have values of 1/2, 3/2, 2 and 3, depending on the nature of the electronic transition responsible for absorption, p is equal to1/2 for allowed direct transitions, 3/2 for direct forbidden transitions, 2 for allowed indirect transitions and 3 for forbidden indirect transitions. For amorphous materials, indirect transitions are valid according to the Tauc relations [40], i.e., the power part $p = 2$; so, the values of indirect optical band gap energy E_{opt} can be obtained from Expression (6) by extrapolating the absorption coefficient to zero absorption in the $(\alpha\hbar\omega)^{1/2}$ vs $\hbar\omega$ plot, as shown in Fig. 8. The respective values of E_{opt} are obtained by extrapolating $(\alpha\hbar\omega)^{1/2} = 0$ for the indirect transitions [40,41]. The values of the E_{opt} for the glass samples are presented in Table 2. It is observed from Table 2 that the values of optical band gap (E_{opt}) decreases from 2.47 eV to 2.01 eV, as the content of WO_3–Ag_2O increases from 15 to 60 mol%. These E_{opt} values are also in reasonable agreement with the optical band gap values found in other tellurite glasses [42–44]. The increasing incorporation of WO_3–Ag_2O is mainly responsible for the E_{opt} diminishing.

From the Raman spectra analysis, it is clear that the addition of WO_3–Ag_2O content to the TeO_2 network leads to the formation of NBOs in the form of $Te{-}_{eq}O^-Ag^+$, $Te{-}_{ax}O^-Ag^+$, $W{-}O^-Ag^+$, W=O and also Te=O. Hence increase in WO_3–Ag_2O content results in progressive creation of NBOs at the expense of bridging oxygen (BO). The NBO which bound an excited electron less tightly than

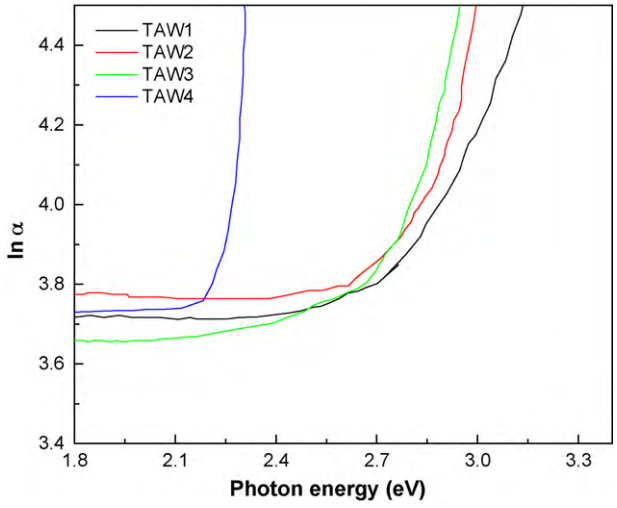

Fig. 9. Urbach plot of TeO_2–Ag_2O–WO_3 glasses.

the BO and NBO is more polarizable than the BO. Thus, creation of NBOs seems to be reason for shift of cut-off wavelength (λ_c) towards higher wavelengths and in turn decreases the E_{opt} values. However, the decrease in E_{opt} by addition of Ag_2O–WO_3 content may also be related to the change in the E_{opt} of constituent oxides (TeO_2 = 3.79 eV, Ag_2O = 1.3 eV, WO_3 = 2.70 eV) [16].

In glass and amorphous materials there exists a band tailing in the forbidden energy band gap. The extent of band tailing is a measure of the disorder in the material and can be estimated using Urbach rule [45].

$$\alpha(\omega) = \alpha_o \exp\left[\frac{\hbar\omega}{\Delta E}\right] \tag{7}$$

where α_o is constant and ΔE is the width of the band tails of electron states in the forbidden band gap and which is also known as the Urbach energy. This relation was first proposed by Urbach to describe the absorption edge in alkali halide crystals [45]. Fig. 9 shows the variation of lnα with photon energy ($\hbar\omega$) for present glass system (Urbach plot). The values of Urbach energy (ΔE) were calculated from the reciprocal of the slope of the linear region of the curves and are presented in Table 2. It is found that ΔE lie in the range of 0.37–0.15 eV, decreases with increase of WO_3–Ag_2O content. The least Urbach energy (ΔE = 0.15 eV) is observed for TAW4 glass. This suggests that the degree of disorder of present glasses decreases with WO_3–Ag_2O content.

3.4.2. Theoretical optical basicity (Λ_{th}) and refractive index (n)

The theoretical optical basicity (Λ_{th}) for the glass system under study has been calculated using following equation which is based on the approach proposed by Duffy and Ingram [46].

$$\Lambda_{th} = X(TeO_2)\Lambda(TeO_2) + X(Ag_2O)\Lambda(Ag_2O) + X(WO_3)\Lambda(WO_3)$$

where $X(TeO_2)$, $X(Ag_2O)$, $X(WO_3)$ are the equivalent fractions of the different oxides, i.e., the proportion of the oxide atom they contribute to the glass system and $\Lambda(TeO_2)$, $\Lambda(Ag_2O)$ and $\Lambda(WO_3)$ are optical basicity values assigned to the constituent oxides. Here the values of $\Lambda(TeO_2)$ = 0.96, $\Lambda(Ag_2O)$ = 0.441 and $\Lambda(WO_3)$ = 1.04 have been taken from literature [16,47]. The Λ_{th} values calculated using above equation for the present system are given in Table 2. It can be seen from Table 2 that the values of Λ_{th}, for the present system lie between 0.927 and 0.828.

The relationship between the refractive index (n) and the optical band gap (E_{opt}) was examined by the relationship [16].

$$\left(\frac{n^2-1}{n^2+2}\right) = 1 - \sqrt{\frac{E_{opt}}{20}} \tag{8}$$

The refractive index (n) values calculated using above equation for the present system are given in Table 2. It is observed from Table 2 that the refractive index (n) increases from 2.55 to 2.73 with an increase in the WO_3–Ag_2O content. The increase in the refractive index (n) depends on some of the following factors such as (i) from Raman analysis, it is shown that more NBOs are created with WO_3–Ag_2O content, these NBOs creates more ionic bonds, which manifest themselves in a larger polarizability over the covalent bonds of BOs, providing a higher refractive index value. (ii) The increase in density and molar volume are related to the increase in refractive index. (iii) The increase in refractive index may also be related the lower cation polarizability of W^{6+} ions (0.147 Å^3), compared with cation polarizability of Te^{4+} ions (1.595 Å^3) [48].

4. Conclusions

Transparent and stable glasses were obtained in the TeO_2–Ag_2O–WO_3 system. The physical and optical properties of present system are affected by the changes in the glass composition. The Raman analysis shows that addition of WO_3–Ag_2O to TeO_2 glass matrix results in the formation of W–O^-Ag^+, W–O–Te, Te–$_{eq}O^-Ag^+$, Te–$_{ax}O^-Ag^+$, Te=O and W=O species, while that of the Te–O–Te linkages decreases as WO_3–Ag_2O increases. The density, molar volume and oxygen molar volume values increases with the WO_3–Ag_2O content. The values of n_b, $\overline{n_c}$, $\overline{F}$ and OPD decreases with increasing the content of Ag_2O–WO_3, which is in agreement with the decrease in T_g. The optical band gap (E_{opt}) (2.47–2.01 eV), Urbach energy (ΔE) values (0.37–0.15 eV) decreases and the refractive index (n) values (2.55–2.73) increases with WO_3–Ag_2O content.

Acknowledgements

One of the authors, G. Upender is grateful to UGC (University Grants Commission), New Delhi, for providing financial assistance under the scheme of RFSMS (Research Fellowships in Sciences for Meritorious Students).

References

[1] D. Lezal, T. Bludska, J. Horak, A. Sklenar, S. Karamazoo, M. Vlcek, Phys. Chem. Glasses 43 (2002) 296.
[2] J. Zhang, J. Qiu, Y. Kawamoto, Mater. Lett. 55 (2002) 77.
[3] Y. Ding, S. Jiang, B.C. Hwang, T. Luo, N. Peyghambarian, Y. Himei, T. Ito, Y. Miura, Opt. Mater. 15 (2000) 381.
[4] K. Sae-Hoon, Y. Toshinobu, J. Am. Ceram. Soc. 78 (1995) 106.
[5] M. Tatsumisago, T. Minami, Ceramics 28 (1993) 1227.
[6] J.S. Wang, E.M. Vogel, E. Snitzer, Opt. Mater. 3 (1994) 187.
[7] J. Lin, W. Huang, Z. Sun, C.S. Ray, D.E. Day, J. Non-Cryst. Solids 336 (2004) 189.
[8] J.E. Stanworth, J. Soc. Glass Technol. 36 (1952) 217.
[9] T. Kosuge, Y. Benino, V. Dimitrov, R. Sato, T. Komatsu, J. Non-Cryst. Solids 242 (1998) 154.
[10] I. Shaltout, Y. Tang, R. Braunstein, E.E. Shaisha, J. Phys. Chem. Solids 57 (1996) 1223.
[11] M.J. Waber, J.D. Meyers, D.H. Blackburn, J. Appl. Phys. 52 (1981) 2944.
[12] J.E. Stanworth, Nature 169 (1952) 581.
[13] R.A. El-Mallawany, Tellurite Glasses Handbook – Physical Properties and Data, CRC Press, Boca Raton, FL, 2002.
[14] G. Upender, Suresh Bharadwaj, A.M. Awasthi, V. Chandra Mouli, Mater. Chem. Phys. 118 (2009) 298.
[15] G. Upender, Vasant G. Sathe, V. Chandra Mouli, Phys. Chem. Glasses 50 (2009) 399.
[16] V. Dimitrov, S. Sakka, J. Appl. Phys. 79 (3) (1996) 1736.
[17] B.V.R. Chowdari, P. Pramoda Kumari, J. Mater. Sci. 33 (1998) 3591.
[18] Y. Wang, S. Dai, F. Chen, T. Xu, Q. Nie, Mater. Chem. Phys. 113 (2009) 407.
[19] Y. Saddeek, L. Abd El Latif, Physica B 348 (2004) 475.

[20] S. Bale, N. Srinivas Rao, Syed Rahman, Solid State Sci. 10 (2008) 326.
[21] R.C. West, M.J. Astle, W.H. Beyer, (Eds.), Handbook of Chemistry and Physics, CRC, Boca Raton, FL, Section F-157, 1987.
[22] J.A. Kerr, CRC Handbook of Chemistry and Physics, CRC Press, FL, 2000.
[23] B.V.R. Chowdari, P. Pramoda Kumari, Solid State Ionics 113–115 (1998) 665.
[24] B. Bridge, A.A. Higazy, Phys. Chem. Glasses 27 (1) (1986) 1.
[25] B. Bridge, Phys. Chem. Glasses 28 (1987) 70.
[26] E. Lambson, G. Saunders, B. Bridge, R.A. El-Mallawany, J. Non-Cryst. Solids 69 (1984) 117.
[27] R.A. El-Mallawany, Mater. Chem. Phys. 63 (2000) 109.
[28] S.R. Elliott, Physics of Amorphous Materials, Longman Scientific & Technical, London, 1990.
[29] I. Shaltout, Y.I. Tang, R. Braunstein, A.M. Abu-Elazm, J. Phys. Chem. Solids 56 (1995) 141.
[30] C.Y. Zahra, A.M. Zahra, J. Non-Cryst. Solids 190 (1995) 251.
[31] Y. Dimitriev, Y. Ivanova, M. Dimitrova, E.D. Lefterova, P.V. Angelov, J. Mater. Sci. Lett. 19 (2000) 1513.
[32] V.O. Sokolov, V.G. Plotnichenko, V.V. Koltashev, E.M. Dianov, J. Non-Cryst. Solids 352 (2006) 5618.
[33] J. Ozdanova, H. Ticha, L. Tichy, J. Non-Cryst. Solids 353 (2007) 2799.
[34] J. Ozdanova, H. Ticha, L. Tichy, J. Non-Cryst. Solids 355 (2009) 2318.
[35] C.Y. Wang, Z.X. Shen, B.V.R. Chowdari, J. Raman Spectrosc. 29 (1998) 819.
[36] H. Burger, K. Kneipp, H. Hobert, W. Vogel, K. Kozhukharov, S. Neov, J. Non-Cryst. Solids 151 (1992) 134.
[37] T. Sekiya, N. Machida, S. Ogawa, J. Non-Cryst. Solids 176 (1994) 105.
[38] R.H. Sands, Phys. Rev. 99 (1995) 1222.
[39] E.A. Davis, N.F. Mott, Philos. Mag. 22 (1970) 903.
[40] J. Tauc, Amorphous and Liquid Semiconductor, Plenum Press, NY, 1974.
[41] J. Pankove, Optical Processes in Semiconductors, Prentice-Hall, Englewood Cliffs, NJ, 1971.
[42] S. Al-Ani, C.A. Hogarth, R.A. El-Mallawany, J. Mater. Sci. 20 (1985) 661.
[43] Yousef El Sayed, J. Phys. D: Appl. Phys. 38 (2005) 3970.
[44] R.A. El-Mallawany, M.D. Abdalla, I.A. Ahmed, Mater. Chem. Phys. 109 (2008) 291.
[45] F. Urbach, Phys. Rev. 92 (1953) 1324.
[46] J.A. Duffy, M.D. Ingram, in: D. Uhlman, N. Kreidl (Eds.), Optical Properties of Glasses, American Ceramic Society, Westerville, 1991.
[47] T. Wakasugi, A. Ohkawa, K. Tanaka, R. Ota, J. Non-Cryst. Solids 298 (2002) 252.
[48] V. Dimitrov, T. Komatsu, J. Solid State Chem. 178 (2005) 831.